

TWO-DIMENSIONAL HYDRODYNAMIC SIMULATIONS OF CONVECTION IN RADIATION-DOMINATED ACCRETION DISKS

ERIC AGOL (CHANDRA FELLOW)

Physics and Astronomy Department, Johns Hopkins University, Baltimore MD 21218 and Theoretical Astrophysics, Caltech MS 130-33, Pasadena, CA 91125

JULIAN KROLIK

Physics and Astronomy Department, Johns Hopkins University, Baltimore, MD 21218

NEAL J. TURNER & JAMES M. STONE

Astronomy Department, University of Maryland, College Park, MD 20742

Draft version October 28, 2018

ABSTRACT

The standard equilibrium for radiation-dominated accretion disks has long been known to be viscously, thermally, and convectively unstable, but the nonlinear development of these instabilities—hence the actual state of such disks—has not yet been identified. By performing local two-dimensional hydrodynamic simulations of disks, we demonstrate that convective motions can release heat sufficiently rapidly as to substantially alter the vertical structure of the disk. If the dissipation rate within a vertical column is proportional to its mass, the disk settles into a new configuration thinner by a factor of two than the standard radiation-supported equilibrium. If, on the other hand, the vertically-integrated dissipation rate is proportional to the vertically-integrated total pressure, the disk is subject to the well-known thermal instability. Convection, however, biases the development of this instability toward collapse. The end result of such a collapse is a gas pressure-dominated equilibrium at the original column density.

Subject headings: accretion, accretion disks, convection

1. INTRODUCTION

More than twenty-five years ago, Shakura & Sunyaev (1973, hereafter SS) showed that the inner portions of accretion disks with luminosities near Eddington are likely to be dominated by radiation pressure. Because the vertical component of gravity increases $\propto z$ near the disk mid-plane, true vertical hydrodynamic equilibrium could only be achieved if the heating rate is constant with height. If the physical dissipation rate scales locally with the density, then hydrostatic and radiative equilibrium require the gas density to be constant from the disk midplane to the disk surface.

Unfortunately, this equilibrium is subject to numerous instabilities. Lightman & Eardley (1974) pointed out that if the viscous stress is proportional to the radiation pressure, perturbations to the surface density grow on the (comparatively long) viscous inflow timescale. Shakura & Sunyaev (1976) then observed that in these same conditions the thermal content of the disk is likewise unstable, with a growth time comparable to the (shorter) thermal timescale. Bisnovatyi-Kogan & Blinnikov (1977, hereafter BKB) noticed that if the radiation is locked to the gas even on short length scales (i.e., if, for the purpose of dynamics, the optical depth is treated as effectively infinite), such disks should be convectively unstable, for the specific entropy decreases upward (the radiation pressure decreases upward while the density is constant); the linear growth rate for convective “bubbles” was worked out by Lominadze & Chagelishvili (1984). This work has been recently extended by Pietrini & Krolik (2000), who derived a hydrodynamic WKB dispersion relation in the presence of rotation and including the effects of finite optical depth. In other recent work, Gammie (1998) demonstrated that

a magnetic field in radiation-supported disks can catalyze a short-wavelength ($kH \gg 1$, where H is the disk scale height) overstable wave mode. Blaes & Socrates (2000) found the dispersion relation for radiation MHD modes within radiation-dominated disks.

With so many instabilities potentially operating, one must wonder what is the real state of these disks. Numerous suggestions exist in the literature. BKB argued that the disk structure could be determined by imposing the conditions of constant specific entropy (a state achieved as a result of convection) and hydrostatic equilibrium. Liang (1977) defined a new equilibrium by parameterizing the efficiency of convective heat transport. Shakura, Sunyaev, & Zilitinkevich (1978) found an analytic solution for the vertical structure based on these same assumptions, but including support from turbulent motions in the hydrostatic equilibrium. They were able to find an analytic solution to the equations granted the assumption that the rms Mach number of the turbulence took a special value. Robertson and Tayler (1981) argued that convection does not quench the thermal instability, making rough estimates for the effect of convection on transport. Others (Cannizzo 1992; Milsom, Chen & Taam 1994; Rozanska et al. 1999) have proposed models based on the “mixing-length” prescription. Eggum et al. (1987), Milsom & Taam (1997), and Fujita & Okuda (1998) used 2-D radiation hydrodynamic simulations to study various aspects of these disks.

Unfortunately, each of these previous attempts to understand the structure of radiation-dominated disks has been lacking in one or more crucial respects. None of the analytic efforts actually solved the force equation without making some assumption about the character of the answer, while none of the numerical simulations had the

resolution to actually determine the internal vertical structure (these simulations were primarily aimed at exploring issues involving the global behavior of disks rather than the particulars of vertical structure).

The object of the work presented here is to use radiation hydrodynamic simulations to focus on the vertical equilibrium of radiation-dominated disks so that one may actually determine the structure of bright accretion disks in the range of radii where they release most of their energy, their innermost rings. In addition to the intrinsic interest of this effort for deepening our understanding of accretion dynamics, solving this question is a prerequisite for any effort to predict the spectrum of radiation emerging from these disks—the nature of the disk atmosphere, and therefore the character of any features imprinted on the spectrum in the disk photosphere, depends crucially on the vertical distribution of gas density and heat deposition. Though the viscous mechanism operating in accretion flows is likely due to magnetic stresses, we parameterize the effects of viscosity so as to use a simpler hydrodynamic code.

2. SIMULATION METHODS

The tool we employ is the Zeus simulation code (Stone & Norman 1992) with its flux-limited radiation diffusion module (Turner & Stone 2001). This code solves five coupled partial differential equations on a fixed Eulerian grid: the mass-continuity equation, the Navier-Stokes equation, the energy conservation equations for both the gas and the radiation, and the radiation momentum conservation equation. Defining the radiation quantities in a cylindrical coordinate frame comoving with the fluid, and retaining only those terms first order in v/c , these equations are:

$$\frac{D\rho}{Dt} + \rho \nabla \cdot \mathbf{v} = 0, \quad (1)$$

$$\rho \frac{D\mathbf{v}}{Dt} = -\nabla p + \frac{1}{c} \kappa \rho \mathbf{F} - \rho \Omega^2 z \mathbf{z} - 2\rho \Omega (v_\phi - r_o \Omega) \mathbf{r} + 2\rho \Omega v_r \boldsymbol{\phi} + 3\rho \Omega^2 (r - r_o) \mathbf{r}, \quad (2)$$

$$\rho \frac{D}{Dt} \left(\frac{E}{\rho} \right) = -\nabla \cdot \mathbf{F} - \nabla \mathbf{v} : \mathbf{P} + 4\pi \kappa_P \rho B - c \kappa_E \rho E + \eta, \quad (3)$$

$$\rho \frac{D}{Dt} \left(\frac{e}{\rho} \right) = -p \nabla \cdot \mathbf{v} - 4\pi \kappa_P \rho B + c \kappa_E \rho E, \quad (4)$$

and

$$\frac{\rho}{c^2} \frac{D}{Dt} \left(\frac{\mathbf{F}}{\rho} \right) = -\nabla \cdot \mathbf{P} - \frac{1}{c} \kappa \rho \mathbf{F}. \quad (5)$$

Here the convective derivative $D/Dt \equiv \partial/\partial t + \mathbf{v} \cdot \nabla$. The unit vectors in the radial, azimuthal, and vertical directions are \mathbf{r} , $\boldsymbol{\phi}$, and \mathbf{z} , respectively. The quantities ρ , e , \mathbf{v} , and p are the gas mass density, energy density, velocity, and pressure respectively, while E , \mathbf{F} , and \mathbf{P} are the radiation energy density, momentum density or flux, and pressure tensor, respectively. Only absorptive opacity is included in the Planck mean opacity κ_P and the energy mean opacity κ_E , but scattering is added to absorption in the flux-mean total opacity κ . Energy injection is permitted via the function η (see later discussion). The orbital frequency, $\Omega = \sqrt{GM/r_o^3}$, is evaluated at the central radius r_o . The disk is assumed to be azimuthally symmetric,

and shearing-box coordinates (the Hill potential) are used to describe the gravity (the Ω -dependent terms in equation 2 all arise from this approximation to the potential in rotating coordinates).

The mass-continuity and Navier-Stokes equations are advanced in time using operator-splitting. The radiation transport problem is solved implicitly using the approximation of flux-limited diffusion (Turner & Stone 2001). The code assumes a gas equation of state with e , the gas energy density, evolved adiabatically, but including absorption and emission of radiation. The gas pressure is defined as $p_{gas} = (\gamma - 1)e$, with $\gamma = 5/3$.

In all our simulations, the problem area was a radial segment of a geometrically-thin, optically-thick, radiation-dominated accretion disk. In terms of the disk height, $H = F_o \kappa_F / (c \Omega^2)$ as predicted by the SS equilibrium, where $F_o = 3\Omega^2 \dot{M} / (8\pi)$ is the radiation flux at the top of the disk, c is the speed of light, we simulated the dynamics in a region stretching in the vertical direction from $z = -2H$ to $z = 2H$, and in the (cylindrical) radial direction from $r = r_o - 2H$ to $r = r_o + 2H$. Two values of central radius r_o were chosen, $100r_g$ and $200r_g$, where $r_g = GM/c^2$. The black hole mass was $10^8 M_\odot$, and we set the accretion rate at $\dot{M} = (3 - 10) \times 10^{25} \text{ gm s}^{-1}$, appropriate for bright active galactic nuclei shining at (20-60)% of the Eddington limit.

The initial condition in every case was a slightly-modified SS equilibrium. Because that equilibrium becomes ill-defined at the disk surface (where it predicts that the gas density falls discontinuously to zero), we constructed a more complete version of the same equilibrium allowing for the small amount of gas pressure support that exists at the top. In this initial equilibrium (but not in our simulations), we assume that $T_{gas} = T_{rad}$ locally throughout the disk. Fixing the flux, F_o , column density, Σ , and orbital frequency, Ω , we used a shooting method to solve simultaneously the hydrostatic equilibrium equation,

$$-\frac{d(p_{gas} + p_{rad})}{dz} = \rho \Omega^2 z, \quad (6)$$

the radiative equilibrium equation,

$$\frac{dF}{dz} = \frac{2F_o \rho}{\Sigma}, \quad (7)$$

and the radiation diffusion equation,

$$F = -\frac{c}{(\kappa \rho + \alpha_o)} \frac{dp_{rad}}{dz}. \quad (8)$$

We introduced an scattering opacity floor, α_o , to prevent the opacity from ever becoming small enough to undercut the validity of the diffusion approximation (see further discussion below). The gas density in this solution is very nearly constant from $z = 0$ almost to $z = H$; starting from just below $z = H$, it falls steeply, but not discontinuously, as z increases. The radial and vertical velocity components were set to zero initially, while the azimuthal velocity components were set to the shearing sheet value, $-1.5\Omega(r - r_o)$.

The column density of the accretion disk at the start of the simulation is chosen to be the value in the the SS equilibrium. Ignoring relativistic correction factors and the correction factor accounting for the outward angular momentum flux, it is

$$\Sigma = \frac{4}{3\kappa\alpha} \dot{m}^{-1} x^{3/2}, \quad (9)$$

where \dot{m} is the accretion rate in Eddington units (for unit efficiency), α is the ratio of the viscous stress to the pressure, Σ has units gm cm^{-2} , and $x = rc^2/GM$. In all but one special case, we fixed α at 0.01 for computing the surface mass density at the start of the simulation.

At the top and bottom edges ($z = \pm 2H$), the boundary condition was chosen to be outflow; that is, fluid quantities in the cells adjacent to the problem area were set equal to the boundary values. In addition, anywhere we set an outflow boundary condition we required the velocity to be outwards; if not, it was set to zero. In the radial direction, periodic boundary conditions were assumed in all quantities except v_ϕ , for which periodicity was enforced for the quantity $v_\phi - v_{Keplerian}$.

The scattering opacity was taken to be the electron scattering value $\kappa_{es} = 0.4 \text{cm}^2 \text{gm}^{-1}$, with certain exceptions. When regions of the simulation zone were optically thin, we found that the diffusion routine took many steps to converge, greatly slowing progress of the code. In addition, the outflow boundary condition for optically-thin flux-limited diffusion was impossible to implement due to a steep density gradient and uniform radiation field near the boundary where the disk has very low density but is nonetheless gas pressure supported. To avoid these difficulties associated with optically-thin radiation transfer, an opacity floor was chosen such that the scattering optical depth across each cell was at least unity (α_o was $2 \times 10^{-12} \text{cm}^{-1}$ for simulation 1 and $2 \times 10^{-13} \text{cm}^{-1}$ for simulation 1). This adjustment of the opacity affected about half of the simulation region, but a much smaller fraction of the total mass. It caused the radiative flux through the upper and lower boundaries to be carried advectively with the fluid rather than by diffusion relative to the fluid; this forced outflow through the outer boundaries, maintaining consistency with our outflow boundary condition. Over a characteristic thermal time for the Shakura-Sunyaev equilibrium

$$t_{thermal} \equiv F_o^{-1} \int_0^H (E + e) dz = H\kappa\Sigma/c \simeq 4/(\Omega\alpha), \quad (10)$$

only a small fraction ($\lesssim 1\%$) of the mass within the simulation region was lost due to outflow. The absorption opacity was assumed to be purely bremsstrahlung: $\kappa_{abs}\rho = 10^{52} \rho^{11/2} e^{-7/2} \text{cm}^{-1}$, where ρ is the mass density and e is the gas energy density.

Without creation of new photons, flux lost out of the top of the disk would ultimately deplete the disk of radiation. In a real disk, new photons are created in a way that depends on the local gas density, temperature, and magnetic field. Here we wish merely to model the radiation process in a phenomenological fashion. To this end, we simply call the local radiation rate η (units of $\text{erg cm}^{-3} \text{s}^{-1}$) and define it by either of two prescriptions: in one case, $\eta \propto \rho$, while in the other η is proportional to the total pressure averaged over the simulation region, but locally proportional to the gas density within any given cell. The former choice was meant to mimic the assumption underlying the SS vertical equilibrium. The latter choice is based, of course, on the thought that the stress is proportional to the total pressure.

Ultimately, the energy for these new photons comes from dissipation of gas motions (and, in a real disk, resistive dissipation of magnetic field energy). However, there is

no clear-cut way to connect photon creation to local viscosity. For example, if, as seems likely, most of the angular momentum transport in disks is due not to something that behaves like viscosity, but rather to MHD turbulence (Balbus & Hawley 1998), there is no simple, local connection between stress and heating, much less between stress and radiation. Consequently, we do not place any viscous counterpart to the radiation creation term η in the gas momentum and energy equations.

The final item to be noted in specifying the simulations is the resolution. The results we present were done with a 128×128 grid, but we reran part of simulation 1 with resolutions of 64×64 and 256×256 to check for convergence. In those cases in which the disk collapsed as a result of thermal instability, we stopped the simulation when nearly all the disk mass was contained within then central 1/4 of the vertical coordinate. At that point, the central half (in both radial and vertical directions) was rebinned to twice the resolution, and the simulation was then restarted.

The simulations and their characteristics are listed in table 2. The three parameters varied were the radius, \dot{M} , and resolution; the radius and \dot{M} change the optical depth as described by equation 9, and also change the ratio of p_{rad}/p_{gas} . Each simulation consisted of two successive phases:

A) The disk was first allowed to come to a statistically steady equilibrium modified by convection with the integrated heating rate fixed globally, but scaled locally with the density, $\eta = F_o\rho/\Sigma$. This readjustment took several thermal times.

B) The heating rate was then allowed to vary in proportion to the average total pressure (“ α ” prescription) to search for possible thermal instability. In this case

$$\eta = \frac{F_o\rho\langle p \rangle}{\Sigma\langle p_o \rangle}, \quad (11)$$

where $\langle p_o \rangle$ is the volume averaged pressure at the end of Phase A.

Table 1: Simulation Parameters

| N | \dot{M} (g/s) | r/r_g | Res. | 4H (cm) | ϕ_{rad} | ϕ_{gas} | α_o |
|---|-----------------|---------|------------------|---------|--------------|--------------|------------|
| 1 | 3.E25 | 100 | 128 ² | 2.4E13 | 95 | 0.50 | 2.E-12 |
| 2 | 1.E26 | 200 | 128 ² | 1.6E14 | 160 | 0.95 | 2.E-13 |

3. READJUSTMENT BY CONVECTION

In this section we discuss the results from Phase A of the simulations.

3.1. Approximate Analytic Description of the Time-Steady State

To provide a context for the simulation results, we begin by discussing how one might find approximate analytic solutions for the vertical structure of radiation-dominated disks. Because the inflow time is very long compared to the dynamical time, $t_{dyn} = 2\pi\Omega^{-1}$, one might expect the disks to be in hydrostatic equilibrium. In the absence of convection, one would also expect the heat flux to be carried by photon diffusion.

On the other hand, when convection is active, one might estimate the heat flux in terms of mixing-length theory (e.g., as described in Clayton 1968). If one could define an effective

mixing-length l , the fraction of the heat carried by convection is

$$F_{conv}/F_o = 13(z/h)^{-1/2}(l/h)^2(\alpha/0.01)(h\Delta\nabla \ln T)^{3/2}, \quad (12)$$

where $\Delta\nabla \ln T$ is the difference between the true logarithmic temperature gradient and the adiabatic temperature gradient. To the degree that convection is efficient, entropy gradients are erased, so that the disk becomes nearly isentropic.

Thus, one way to approximately determine the structure of these disks is to require all three of these conditions: hydrostatic balance, isentropy, and photon diffusive equilibrium (or at least that photon diffusion carry a specified fraction of the heat). However, this is impossible because any two of these three conditions suffice to determine the structure of the disk. For example, SS applied the two conditions of hydrostatic equilibrium and photon diffusive equilibrium, without reference to the condition of isentropy (in fact, their equilibrium, as we have already remarked, has a strongly unstable entropy gradient). In this solution, the density is constant with altitude up to H , and drops sharply to zero for $z > H$. Thus, the mass-weighted average height of the disk is $\langle z \rangle \equiv \int_0^H \rho z dz / \int_0^H \rho dz \sim H/2$.

Similarly, BKB assumed hydrostatic balance and isentropy, but made no assumption with regard to radiative balance. If the turbulence is subsonic, then this approximation is appropriate since the turbulent pressure will be much smaller than the radiation pressure. Then, the diffusive flux is simply

$$F_{dif} = F_o z/H. \quad (13)$$

The density distribution they found is:

$$\rho = \rho_c \left[1 - \left(\frac{z}{H} \right)^2 \right]^3, \quad (14)$$

where ρ_c is the central density, given by

$$\rho_c = \frac{35\Sigma}{32H}. \quad (15)$$

The mass-weighted average height of this disk is $\langle z \rangle = 35H/128$, about half that of the SS solution. The specific entropy, $s = \frac{4}{3}a^{1/4}E^{3/4}/\rho$, is found to be

$$s = \left(\frac{2}{105^{1/4}} \right) \left[\frac{a\kappa^7 F_o^7}{\Sigma\Omega^8 c^7} \right]^{1/4}. \quad (16)$$

In this case, if the dissipation is proportional to density, then the convective flux is

$$F_{con} = \frac{35}{16}F_o\zeta \left(\frac{19}{35} - \zeta^2 + \frac{3}{5}\zeta^4 - \zeta^6/7 \right) \quad (17)$$

where $\zeta = z/H$. Thus, for small ζ , the ratio of the convective flux to the diffusive flux is simply 19/16; i.e. the convective flux is always comparable to the diffusive flux. At $\zeta = 1$, $F_{con} = 0$ so all the radiation escapes diffusively. The volume-integrated radiation energy in the disk is reduced by a factor of 3 with respect to the SS solution, so the thermal timescale is decreased by the same factor.

Alternatively, one could also insist that the specific entropy is constant and that the disk be in radiative balance but pay no attention to hydrostatic equilibrium (this assumes that the convective flux is small compared to the diffusive flux). In that case, if the dissipation is proportional to density, then the density profile would be

$$\rho = \rho_c \text{cn}^3 \left[\frac{\sqrt{2}\rho_c z}{\Sigma} \middle| \frac{1}{2} \right], \quad (18)$$

where cn is a Jacobi elliptic function and ρ_c is the central density, given by

$$\rho_c = \frac{\sqrt{\pi}\Gamma(1/4)\Sigma}{4\Gamma(3/4)H}. \quad (19)$$

The entropy turns out to be identical to equation 16, except for a different numerical factor in front: $4(4/3)^{1/4}\Gamma(3/4)/\Gamma(1/4)/\sqrt{\pi}$, which is 1.3 times greater than in the BKB solution. The average radiation energy density in this solution is 4 times smaller than in the SS solution. A disk obeying these assumptions would be out of hydrostatic balance by $\rho_c\Omega^2 H(\sqrt{2}\text{dn}(u/2)\text{sn}(u/2) - z/H)$, where $u = \sqrt{2}\rho_c z/\Sigma$, and dn, sn are Jacobi elliptic functions. For hydrostatic equilibrium to exist, turbulence must provide this deficit. The quantity in parentheses can be approximated by $\sim 0.4 \sin \pi(z/H)^{4/5}$, so the turbulent velocity must be of order the sound speed, $\sim H\Omega$.

Thus, at most two of these three plausible conditions can be satisfied exactly. On the other hand, it is possible to approximately satisfy all three if small departures are allowed for each one. Shakura et al. (1978) tried to modify both the hydrostatic balance and energy transport equations to allow for small departures (specifically, the kinetic energy contribution in the hydrostatic equilibrium equation and convective heat transport in the energy equation). However, they were able to find an analytic solution only for the special case in which the rms Mach number $\mathcal{M} = 2/3$. When that is the case, the density distribution is

$$\rho = \rho_c \left[1 - \left(\frac{z}{H} \right)^2 \right], \quad (20)$$

where $\rho_c = 3\Sigma/(4H)$. Unfortunately, there is no particular reason to expect that \mathcal{M} takes this value (in fact, the simulations we performed indicated that it is smaller by an order of magnitude). Consequently, it is necessary to solve the equations of motion numerically in order to find the true compromise between these three conditions that is found in real disks.

3.2. Dynamical readjustment due to convection

We are now ready to report the results of our simulations.

Within the body of the disk, the timescale for thermal equilibration of the radiation and the gas is the shortest timescale; it is a fraction $< 1/20$ of a dynamical timescale. Consequently, deep inside the disk the gas and radiation temperatures quickly become equal. Near the surface, the timescale for radiation to diffuse outwards is comparable to or shorter than the thermal equilibration timescale, so in those regions the gas temperature is anywhere from 10 to 10^3 times greater than the radiation temperature.

Though our initial condition satisfies hydrostatic equilibrium, it is convectively unstable. Pietrini & Krolik (2000) showed that in the WKB approximation (i.e., $kH \gg 1$) the most rapidly growing modes in the linear regime are those whose wave-vectors are nearly horizontal, and that the growth rate for these modes is

$$\Omega_{conv} = \sqrt{\frac{3}{2}}\Omega \left(\frac{z}{H} \right) \left[1 - \left(\frac{z}{H} \right)^2 \right]^{-1/2}, \quad (21)$$

almost independent of wavelength when $\kappa\Sigma \gg 1$ (note the typographical error of a factor of 2 in equation 20 of Pietrini & Krolik). That is, they predicted that convective motions in this equilibrium will grow most rapidly near the surface of the disk, and that the basic growth timescale is the dynamical time. Our simulations confirmed this prediction quantitatively for $z/H \lesssim 1/2$; for example, at 0.4H the analytic growth time

is 9×10^5 s, while the measured growth time in simulation 1 is 10^6 s. However, near the disk surface, the WKB approximation breaks down because there are sharp gradients in density and pressure. As a result, the numerical growth rate we find is slower than the analytic value by a factor of a few near $z \sim H$.

In the non-linear regime, growth is most rapid for longer wavelengths, much as in the case of the Rayleigh-Taylor instability (Garabedian 1957). Horizontal density modulations near the top of the simulated disks with wavelengths of order $H/10$ grow within a few dynamical times of the start of the simulation (Figure 1). Overdense blobs fall, become Kelvin-Helmholtz unstable, and form an inverse-mushroom shape. The disk rapidly becomes turbulent, mixing high and low entropy regions, and then smooths out a bit, while steady convective motions continue.

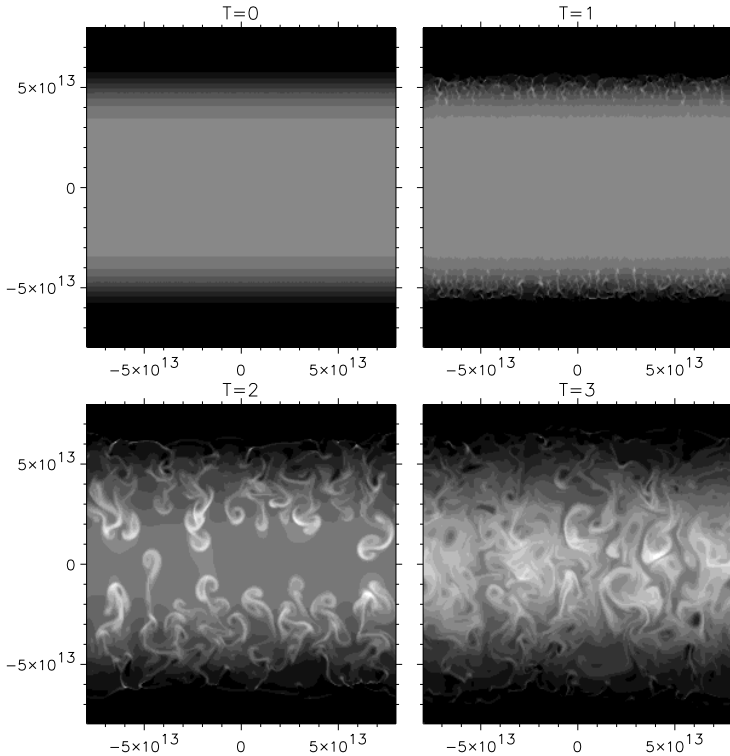


FIG. 1.— The density distribution in simulation 1 (at 256^2 resolution) at times $t/t_{dyn} = 0, 1, 2,$ and 3 . The grey scale is linear from $\rho = 0$ (black) to $6 \times 10^{-9} \text{ gm cm}^{-3}$ (white). The horizontal axis is radial distance from the central radius of the simulation, the vertical axis is altitude from the disk midplane; both are in cm.

After ~ 90 dynamical times, the disk achieves an approximate statistical steady-state. Convection continues to occur, creating small-amplitude fluctuations, but average properties remain very nearly constant. The outgoing flux at the top of the box fluctuates about the mean heating rate, evidence that the simulation has reached a steady state. Several stable convective cells are formed, in which low entropy sinking regions of size $\sim H$ are surrounded by upwelling plumes with twice the entropy (Figure 2; to be precise, at any given height within the body of the disk, the specific entropy in the plumes is roughly twice the lowest specific entropy elsewhere in the disk at that height). The plumes are not completely resolved since at their narrowest in the midplane, they are only spanned by 2 pixels. If the heating rate is proportional to the local density, mean conditions in the disk remain constant for the duration of Phase A of the simulation, 11 initial thermal times, or 180 dynamical times. In contrast to the “square-wave” density pro-

file of the initial equilibrium, the mean density profile exhibits a smooth fall from the midplane out to the top. The mass-weighted average height of the disk changes by a factor of ~ 2 as convection carries more flux outwards, reducing the radiation pressure, causing the disk to collapse. The reduced height further reduces the thermal time, causing more flux to escape, and further collapse until radiation pressure supports the disk again. At the end of the readjustment process, the volume-integrated radiation energy is reduced relative to what it was in the initial equilibrium by a factor of 4.4 and 4.6 in simulations 1 and 2, respectively. This factor is slightly larger than the factor of 3 predicted by the analytic BKB scaling, but is close to the factor of 4 predicted by equation 18. We reran simulation 1 at lower (64^2) and higher resolution (256^2) to check for convergence. We found that the radiation energy density in the 64^2 simulation disagreed by 20% at the end of phase A, demonstrating that at this resolution the simulation was not converged. At higher resolution, 256^2 , we were only able to run the simulation for about a thermal time since the run time scales as N^4 , but we found that the difference between the total radiation energy density of the 128^2 and 256^2 simulations had a standard deviation of only 0.6%, indicating that the 128^2 simulation was indeed converged. We utilize this higher resolution run when studying the initial convective collapse (e.g. Figure 1).

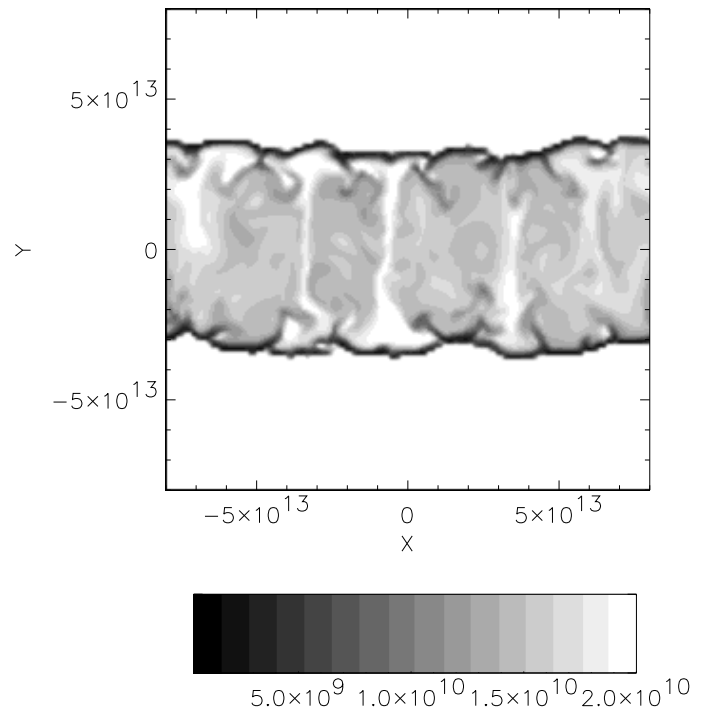


FIG. 2.— The specific radiation entropy distribution in simulation 1 (resolution 128^2) in units of $\text{cm}^2 \text{ s}^{-2} \text{ K}^{-1}$ at $t = 97 t_{dyn}$. Axes are as in Fig. 1; regions above the maximum of the color scale are white.

The mean time-steady density profile of simulation 1, Phase A, is shown in Figure 3, where it is contrasted with the various approximate analytic solutions discussed in the previous subsection. This distribution lies somewhere between the BKB and equation 18 solutions. These analytic solutions break down near the surface where, in actuality, gas pressure support becomes important and LTE no longer holds. We do not find any

dependence of the inner disk structure on the opacity floor (we increased it by a factor of 2 and found the disk structure was identical). The Shakura et al. (1978) solution, with column density equal to the simulation result, deviates significantly from the simulation mean.

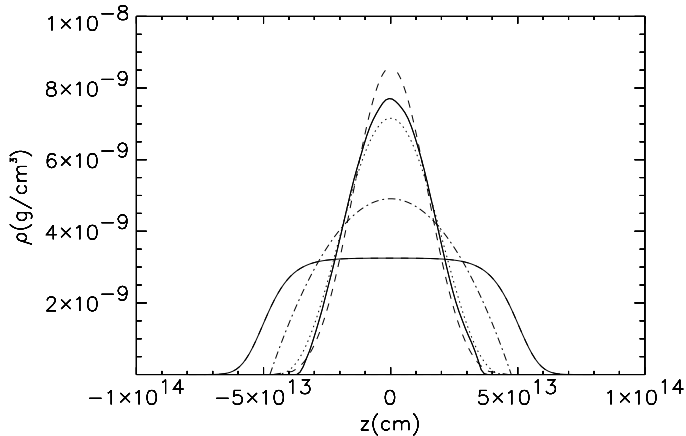


FIG. 3.— Density distribution at $t = 0$ (flat-topped solid line) and $t = 90t_{dyn}$ in simulation 1 (bell-shaped solid line) compared to the prediction of BKB (dotted line), equation 18 (dashed line), and Shakura et al. (1978) (dashed-dot line).

3.3. Heat Transport

The most dramatic feature in Figure 2 is the sharp contrast in specific entropy between rising and sinking regions. Nonetheless, as one might expect from the nonlinear development of an instability that feeds on vertical entropy gradients, convection does an excellent job of smoothing out the radially-averaged specific entropy profile (Figure 4). Within a few dynamical times, the radially-averaged specific entropy in the disk becomes very nearly constant for $z \lesssim 0.8H$; this (on-average) isentropic region contains 98% of the disk mass. Convection is so efficient that this is accomplished with relatively small amplitude motions: the rms Mach number in simulation 1 is $\mathcal{M} \sim 0.1$, vindicating the quasi-hydrostatic approximation made in the BKB solution.

Although the radially-averaged density distribution in the disk is close to that predicted by the two isentropic models (see Fig. 3), the actual value of the mean specific entropy in the disk is about 25% smaller than the analytic prediction (equation 16). This departure may be due to the fact that the entropy is set by the requirement of radiative diffusion matching the total flux at the top of the disk. In the simulations, the density gradient near the disk surface is somewhat different than that predicted by the analytic models because turbulent support becomes comparable to radiation support ($\mathcal{M} \sim 1$). As a result, the entropy necessary to maintain the flux can be slightly different.

This strong turbulence near the disk surface finds its ultimate origin in the reduction in optical depth across convective cells as the density falls sharply near the disk surface. When photons can diffuse across a cell in an eddy turnover time, the radiation does not effectively couple to the fluid, and the sound speed relevant to fluctuations on those lengthscales drops to the (much lower) gas sound speed. Because photon diffusion prevents the radiation from being compressed along with the gas, the gas's compressibility increases dramatically. That permits large local density enhancements, which lead in turn to rapid cell-sinking and high speed motions.

Compressive motions call into play the artificial viscosity em-

ployed in Zeus. In simulation 1, Phase A, dissipation due to artificial viscosity comprises 9% of the total heating rate within the box. In the immediate vicinity of a shock, the dissipation can be significant, but averaged over larger volumes and times, it does not qualitatively alter the disk's thermal properties.

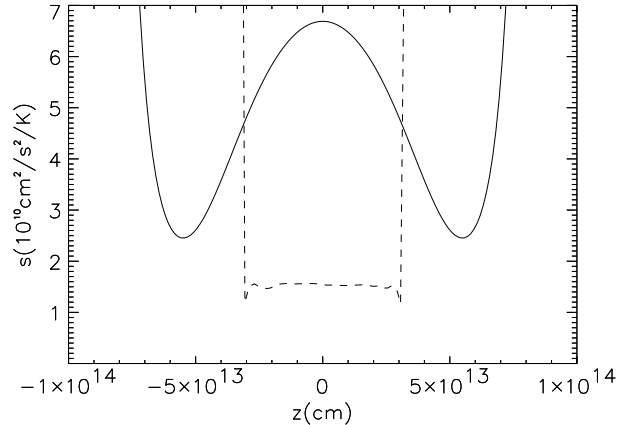


FIG. 4.— Horizontally-averaged entropy as a function of height at $t=0$ (solid line), and at $t = 95t_{dyn}$ (dashed line) from simulation 1.

The mean diffusive flux, $F_{dif} = \langle c\partial_z E / (3\kappa) \rangle$ and the convective flux, $F_{con} = \langle v_z(E + e) + \int_0^z dz (\nabla \cdot \mathbf{P} + p \nabla \cdot \mathbf{v}) \rangle$, averaged radially and in time, are shown in 5. The convective flux is comparable to the diffusive flux near the midplane of the disk, as predicted by the BKB solution. It is, of course, the additional heat loss due to convection that reduces the thermal time so much. In line with intuitive expectation, the diffusive flux rises steadily with height within the disk until it carries almost all the heat at the disk surface. The integrated heating rate and the total flux are nearly equal at the top of the box, indicating that the disk is in quasi-equilibrium.

With these observations in hand, we can evaluate the possible relevance of estimates made through mixing-length theory. On the one hand, the fact that the mean specific entropy is very nearly constant as a function of altitude is consistent with the usual expectation that convection very nearly erases any difference between the actual temperature gradient and the adiabatic temperature gradient. Moreover, our finding that the convective and diffusive heat fluxes are similar deep inside the disk could in principle allow us to turn around equation 12 and evaluate an effective mixing length. However, there are both technical and conceptual problems preventing this. The technical problem is that the limited numerical accuracy with which we can measure the mean temperature gradient will lead to a highly uncertain estimate of the *difference* between it and the very similar adiabatic gradient. The conceptual problem is that the large instantaneous contrasts in specific entropy at fixed altitude demonstrate that the mixing length picture has questionable validity here because the cell sizes are comparable to the entire thickness of the disk.

Above the surface of the disk, the opacity floor that we impose creates a numerical artifact in the character of heat transport. With the true opacity, that region would be optically thin and the heat would be carried almost exclusively by free-streaming radiation; the opacity floor causes the heat to be carried advectively. We believe that this has little consequence for dynamics in the disk body because the region in which the opacity floor is implemented contains only $\sim 1\%$ of the disk mass, and because a simulation with an opacity floor twice as

large gave similar results.

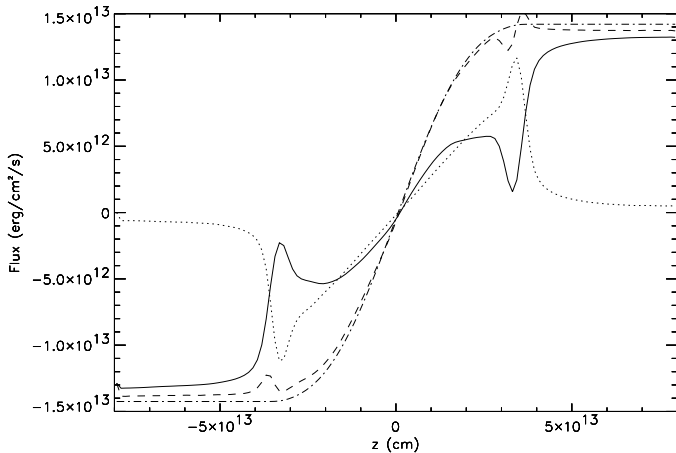


FIG. 5.— Horizontally-averaged diffusive energy flux (dotted line) compared to the convective flux (solid line), total flux (dashed line), and integrated heating rate (dot-dash line) from $t/t_{dyn} = 90$ to 95 in simulation 1. The dominance of convective heat flux for $|z| \gtrsim 4 \times 10^{13}$ cm is an artifact of our opacity floor; in real disks the flux at high altitude is free-streaming.

4. EVOLUTION ON THE THERMAL TIMESCALE

4.1. Thermal Instability

One of the important questions motivating this study is whether the thermal instability predicted on the basis of the α -model actually occurs in radiation-dominated disks. We began this part of our study by verifying that our simulation code reproduced this instability in 1-D when the radiation energy generation rate is proportional to the local radiation energy density. We increased α to 0.1 in this test (only) to reduce the thermal timescale, thereby avoiding a long-term drift in the radiation pressure which occurred only in the 1-D simulations.¹

The growth timescale predicted by Shakura & Sunyaev (1976) in the long-wavelength, radiation-dominated limit is $5(\alpha\Omega)^{-1} = (5/4)t_{therm} \simeq 8t_{dyn}$, numerically equal to 2.5×10^7 s for $\alpha = 0.1$ and $r/r_g = 100$. Our measured growth time was 2.5×10^7 s, a remarkable confirmation of their analytic prediction.

On the other hand, in 2-D, convection becomes possible, so we now describe Phase B of the simulations. To test for thermal instability, the disk was first evolved over several thermal timescales with the heating rate proportional to the total mass (Phase A described in the previous section). We began with this prescription for the heating rather than the α -model for two reasons. First, we wished to separate evolution driven by the convective instability from evolution driven by thermal instability. Second, as a result of the heat lost by convection, the total pressure in the disk after convection sets in is smaller than the initial total pressure. Consequently, if the heating rate is set by proportionality to the total pressure, the proportionality constant that gives thermal balance for the initial disk configuration will not result in enough heating to maintain thermal balance after the convective readjustment. Equation 11 ensures thermal balance at the beginning of Phase B.

¹ The drift is an artifact of the opacity floor. When the radiation flux is purely diffusive, only the radiation energy gradient matters; consequently, the general level of radiation energy density is determined only up to an additive constant. In real disks, the diffusion approximation breaks down in the optically thin region, so it is possible to think of this additive constant as determined by the condition that the flux must be carried by free-streaming radiation at the top of the box. However, in our 1-D simulation the flux is diffusive everywhere due to the opacity floor, so there is nothing in the equations to prevent numerical drifts in the general level of radiation energy density. By contrast, in the 2-D simulations, the flux leaving the box is carried by advection of radiation, which then fixes the radiation normalization as in the free-streaming case.

At the start of Phase B, we first let the thermal instability grow out of numerical noise. Comparing the total radiation energy in the box at the time the heating prescription was changed to α dissipation to the time-averaged radiation energy in the simulations with dissipation proportional to gas density, the integrated numerical fluctuation in the radiation energy was less than 0.1%. In both simulations, as soon as the heating prescription was changed, departures from equilibrium began to grow. The initial growth was well described by an exponential; in simulation 1, its e-folding time was $\sim 18t_{dyn}$, $\simeq 0.9$ thermal times as measured in the convective equilibrium. Simulation 2 showed the same growth time, $\sim 18t_{dyn}$. Because the single-zone linear theory of Shakura & Sunyaev (1976) was specific to their equilibrium, we cannot directly compare this growth time with analytic predictions; however, it is comparable to the thermal time of the collapsed disk, $\sim 16t_{dyn}$. Thus, as predicted by Robertson & Tayler (1981), convection does not quench the thermal instability. However, as we shall see momentarily, it does significantly change its character.

In both simulations, numerical noise lead to disk collapse. However, the pure α -model without convection predicts that the instability has the same growth rate whether the sign of the temperature perturbation is positive or negative. To test whether radiation energy growth can also occur, we reran Phase B with the change that we artificially increased the radiation energy density by 5% at the start. In the $r = 100r_g$ case, the disk still collapsed on a thermal timescale. However, in the $r = 200r_g$ case, the radiation energy density grew on a thermal timescale. The simulation was stopped after most of the mass was lost through outflow from the simulation grid. We speculate that the positive energy perturbation at $r = 100r_g$ was reversed because the initial growth in radiation energy triggered such strong convection that soon the disk was losing more heat than it gained. Because the primary distinction in physical conditions between the two cases was that the ratio of radiation to gas pressure was larger by a factor of 1.7 at $r = 200r_g$ than at $r = 100r_g$, it is possible that their contrary fates were related to this fact. However, we have not been able to convincingly identify any particular diagnostic that enables us to predict which cases will collapse rather than expand despite initially positive temperature perturbations.

We also tried the further experiment of imposing a factor of two increase in the local radiation energy density at the end of Phase A of the $r = 100r_g$ simulation. This had the result of the disk heating and expanding until a significant amount of mass was lost due to strong outflow.

On the basis of these numerical experiments, we conclude that convection biases the development of the thermal instability in the linear regime so that negative radiation energy density perturbations are favored. In some circumstances, this bias is strong enough that even when the initial perturbation is an increase in the radiation energy density, the ultimate result of the instability is collapse. However, this is not always possible, and sufficiently large positive perturbations can overcome convection and lead to runaway growth in the radiation energy density. Our simulations, unfortunately, are not capable of following runaway growth very far because so much of the disk mass is quickly pushed out of the problem area. Consequently, we cannot say how these cases develop in the long-term.

In all these numerical experiments we have restricted ourselves to very simple phenomenological descriptions of the heat-

ing and, in the case of the simulations with imposed perturbations, very simple and uniform perturbations. Real disks undoubtedly behave differently. We regard these simulations therefore as demonstrating that it is possible for thermal instability to occur after convective readjustment when the heating rate is roughly described by the α -model, and that in some circumstances, convection can cause a bias toward collapse. However, these simulations certainly do not provide the final answer to the question of whether and how thermal instability affects physical disks.

4.2. Final state

After the initial exponential collapse, the radiation energy density approaches a constant value as the disk becomes gas-pressure supported and thus thermally stable. This is a consequence of the fact that for fixed surface mass density Σ and fixed stress-parameter α , there exist exactly two thin disk solutions, one radiation-pressure supported with high accretion rate and flux, and one gas-pressure supported with low accretion rate and flux (an advection-dominated solution can also exist, but it is no longer thin). Figure 6 shows the radially averaged gas density in the final state of simulation 1, phase B, while figure 7 shows the radiation and gas pressures. Despite the fact that the gas pressure is larger within the bulk of the disk, p_{rad} becomes larger than p_{gas} near the photosphere simply because the gas density drops precipitously. The density weighted mean of $|z|$ is smaller by a factor of 12.5 at the end of Phase B than at the beginning of Phase A. Twice the grid is rebinned by a factor of two to follow the collapse. We find that the gas becomes strongly clumped in the radial direction filling only $\sim 1/4 - 1/2$ of the simulation region. Since centrifugal forces balance gravity in the radial direction, the clumps remain stable. In a real disk, we expect that viscous stresses will erase this radial stratification.

To illustrate the relationship between the initial radiation-pressure supported state and the final gas-pressure supported state, we explicitly find them in terms of the parameter $\phi = p_{rad}/p_{gas} = (\frac{1}{3}aT^4)/(\rho k_B T/m)$ (m is the average mass per particle). Ignoring the radial clumping, we approximate the disk as a single vertical zone from $z = 0$ to H , writing the hydrostatic equilibrium equation in the form:

$$(1 + \phi)p_{gas} = \rho H^2 \Omega^2. \quad (22)$$

In the α prescription, the radiation equilibrium equation becomes

$$\frac{3}{2}\alpha\Omega(1 + \phi)p_{gas}H = \frac{4c\phi p_{gas}}{\kappa\Sigma}. \quad (23)$$

Defining $\Sigma = 2\rho H$, we solve for ϕ :

$$(1 + \phi)^{10} = \phi^6 \gamma_o \quad (24)$$

where γ_o is defined as

$$\gamma_o = \left(\frac{8c}{3\alpha\kappa_{es}\Sigma}\right)^7 \frac{2am^4}{3\Sigma\Omega k_B^4}. \quad (25)$$

When radiation pressure dominates, $\phi \gg 1$, so $\phi_{rad} \sim \gamma_o^{1/4}$. When gas pressure dominates, if $\phi \ll 0.1$, then $\phi_{gas} \sim \gamma_o^{-1/6}$. Thus, we expect that $\phi_{gas} \sim \phi_{rad}^{-2/3}$. If $\phi_{gas} \sim 1$, then it must be solved for numerically using equation 24.

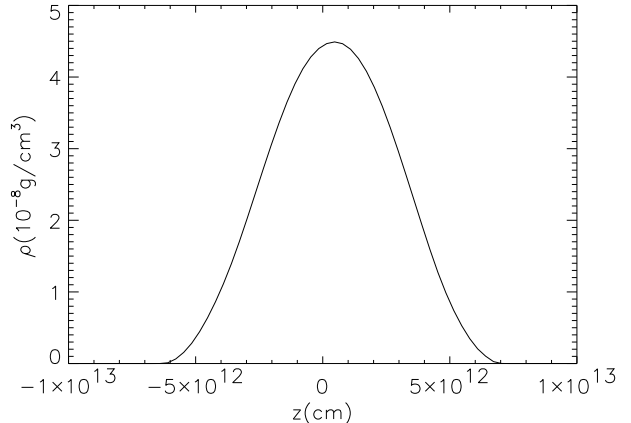


FIG. 6.— Radially-averaged density profile at the end of simulation 1, phase B.

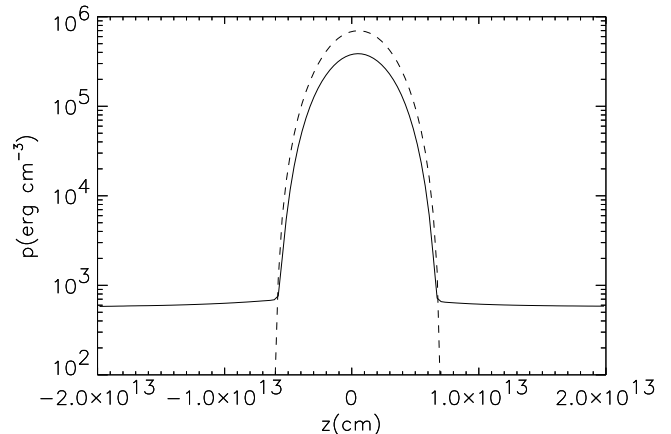


FIG. 7.— Radially-averaged pressure profiles at the end of simulation 1, phase B. Solid line is radiation pressure, while dashed line is gas pressure.

Due to the clumping, this relation is only qualitatively borne out by our simulations. Simulation 1 begins with $\phi_{rad} = 95$ (density-weighted average). As a result of the α renormalization that occurs in order to preserve thermal balance when the heating prescription is changed, α changes from 0.01 to ~ 0.05 (since the radiation pressure is reduced by $\sim 1/5$). With this new value of α , we would expect on the basis of the simple one-zone model just presented that the final ϕ_{gas} after collapse should be ~ 0.9 ; we find 0.54 in simulation 1. Similarly, simulation 2 begins with $\phi = 160$. The effective α again changes from 0.01 to 0.05, leading to a predicted final $\phi_{gas} = 0.38$ (from equation 24); we find $\phi_{gas} \simeq 0.95$. The column density is artificially increased due to the clumping, so the effective $\gamma_o \propto \Sigma^{-8}$ decreases (equation 25), leading to a larger ϕ_{gas} . The radial clumping is much stronger in simulation 2 than in simulation 1, which explains the larger discrepancy. In simulation 2, $p_{rad} \sim p_{gas}$ in the final state, so weak convection is still present.

5. CONCLUSIONS

5.1. Evolution on the dynamical time-scale

We have shown that in a very short time (of order the dynamical time), convection modifies the structure of geometri-

cally thin radiation-dominated disks. Although there are order unity contrasts in specific entropy at fixed altitude z , the radially-averaged entropy becomes very nearly constant with height as a result of convective mixing. The mean density profile that emerges is close to the one predicted in the analytic solution of BKB. As likewise predicted by that analytic solution, the convective flux near the disk midplane is comparable to the diffusive flux. More rapid upward heat flux (for the same dissipation rate) results in smaller mean radiation pressure, weaker support against gravity, and therefore greater mean density. The decreased pressure may cause a further decrease in the viscous stress, resulting in a higher surface mass density and thus lower radiation to gas pressure ratio. One consequence may be that the region of thermal instability is reduced in size by a factor of a few, changing the accretion rate at which near-Eddington disks are subject to thermal instability.

5.2. Evolution on the thermal timescale

We have also shown that evolution on the thermal timescale is quite sensitive to the specific character of the dissipation prescription. Dissipation proportional to density leaves the disk in a long-term statistical equilibrium in which convection and radiative diffusion carry almost equal amounts of energy.

On the other hand, dissipation proportional to vertically-integrated pressure is subject to the thermal instability first pointed out by Shakura & Sunyaev (1976), but subject to a significant modification due to convection: it is biased toward collapse, rather than runaway expansion.

The result of thermal collapse is a new gas pressure-dominated equilibrium at the old column density. The pressure in this new equilibrium is much smaller than in the original one. Because the stress such a disk is capable of exerting (assuming the α model still holds at least approximately, as extensive MHD simulations indicate: Balbus & Hawley 1998) is much smaller than in the initial state, the mass accretion rate through such a disk is much smaller than the initial value. Consequently, if outer regions of the disk continue to pass matter inward at the same rate, mass must build up in the collapsed portions of the disk.

The long-term evolution (i.e., on the inflow timescale) of this situation is difficult to predict. We speculate that the column density will continue to build up until thermal instability sets in at $p_{rad} \sim p_{gas}$. The specific point at which this occurs may be modified by convective heat transport. At this point, the disk no longer has a gas-pressure supported equilibrium available for fixed column density, so the disk may heat up, joining the advection-dominated “slim disk” solution, leading to limit cycle behavior on the inflow timescale (Abramowicz et al. 1988), or convection may lead to episodic release of energy on the dynamical timescale, matching on average the energy dissipated within.

5.3. Future improvements

We have made several assumptions to simplify our calculations that can be tested with future work. First, we have assumed that flux-limited diffusion is an appropriate description of the radiation field. Since our simulations were optically thick everywhere, this may be appropriate, but needs to be checked with a more accurate computation, for example using the variable Eddington factor method described in Stone, Mihalas, & Norman (1992).

Second, we have assumed simple dependences of the heating rate on local disk conditions. Actual disks may have a heating rate which depends on global disk parameters, e.g. height or radius. If a large fraction of the magnetic energy is carried to the corona, then the disk may never become radiation-pressure supported (e.g., as suggested by Svensson & Zdziarski 1994). Simulations of disk annuli indicate that a significant fraction of the magnetic energy generated within an accretion disk can be carried to the corona (Miller & Stone 2000), but not necessarily enough to eliminate a radiation-pressure dominated disk. These simulations need to be extended to include radiation and a physical equation of state to determine the magnitude of the transported energy. Because disks with dissipation primarily at the surface are gas pressure-supported, they are subject to neither convective nor thermal instability.

We believe that the problems of the previous paragraph may best be addressed with 3-D radiation magnetohydrodynamic simulations in which the magnetic field strength and dissipation rate are computed self-consistently. The nature of convective transport as well as the contribution of turbulence to heat transport (Balbus 2000) may have a large effect on our results. Magnetohydrodynamic turbulence might destroy the convective plume structure since the magnetorotational instability operates on the dynamical timescale. The damping of turbulence by radiation diffusion or shocks at the scale αH might determine the heating profile of the disk (Agol & Krolik 1998). If the magnetic stress scales with gas pressure rather than radiation pressure, the thermal instability is suppressed (Piran 1978); whether this is the case can be addressed with radiation MHD simulations. We have purposely limited the scope and detail of our current simulations as our neglect of 3-D magnetohydrodynamics will change the nature of the equilibrium.

We thank Paola Pietrini for very useful discussions. We thank the referee for useful comments which greatly improved the paper. The work of NT and JS was supported by DOE grant DFG0398DP00215. The work of EA and JK was partially supported by NASA Grant NAG 5-3929 and NSF Grant AST-9616922. Partial support for EA was provided by NASA through Chandra Postdoctoral Fellowship grant number PF 0-10013 awarded by the Chandra X-Ray Center, which is operated by the Smithsonian Astrophysical Observatory for NASA under contract NAS8-39073.

REFERENCES

- Abramowicz, M. A., Czerny, B., Lasota, J. P., & Szuszkiewicz, E., 1988, *ApJ*, 332, 646
 Agol, E. & Krolik, J.H. 1998, *ApJ*, 507, 304
 Balbus, S. A., 2000, *ApJ*, 534, 420
 Balbus, S. A. & Hawley, J. F., 1998, *Rev. Mod. Phys.*, 70, 1
 Bisnovatyi-Kogan, G. S. & Blinnikov, J. I., 1977, *A&A*, 59, 111 (BKB)
 Blaes, O. M. & Socrates, A., 2000, *astro-ph/0011097*
 Cannizzo, J., 1992, *ApJ*, 385, 94
 Clayton, D.D. 1968, *Principles of Stellar Evolution and Nucleosynthesis* (New York: McGraw-Hill)
 Eggum, G. E., Coroniti, F. V., & Katz, J. I., 1987, *ApJ*, 323, 634
 Fujita, M. & Okuda, T., 1998, *PASJ*, 50, 639
 Gammie, C. F., 1998, *MNRAS*, 297, 929
 Garabedian, P., 1957, *Proc. Roy. Soc. (London)*, Series A, 241, 423
 Krolik, J. H. 1999, *Active Galactic Nuclei* (Princeton: Princeton Univ. Press)
 Liang, E. P., 1977, *ApJ*, 218, 243
 Lightman, A. P. & Eardley, D. M., 1974, *ApJ*, 187, L1
 Lominadze, D.G. & Chagelishvili, G.D., 1984, *Soviet Astronomy*, 28, 168
 Miller, K. A. & Stone, J. M., 2000 *ApJ*, 534, 398
 Milsom, J. A., Chen, X., & Taam, R. E., 1994, *ApJ*, 421, 668
 Milsom, J. A. & Taam, R. E., 1997, *MNRAS*, 286, 358
 Pietrini, P. and Krolik, J. 2000, *ApJ* 539, 216
 Piran, T., 1978, *ApJ*, 221, 652
 Robertson, J. A. & Tayler, R. J., 1981, *MNRAS*, 196, 185
 Rozanska, A., Czerny, B., Zycki, P. T., & Pojmanski, G., 1999, *MNRAS*, 305, 481
 Shakura, N. I., & Sunyaev, R. A., 1973, *A&A*, 24, 337 (SS)

Shakura, N. I., & Sunyaev, R. A., 1976, MNRAS, 175, 613

Shakura, N. I., Sunyaev, R. A., & Zilitinkevich, S. S., 1978, A & A,
62, 179

Stone, J. M. & Norman, M. L., 1992, ApJS, 80, 753

Stone, J. M., Mihalas, D. & Norman, M. L., 1992, ApJS, 80, 819

Svensson, R. & Zdziarski, A. A., 1994, ApJ, 436, 599

Turner, N. J. & Stone, J. M., 2001, ApJS in press